Journal of Applied Physics

Optical properties of single wurtzite/zinc-blende ZnSe nanowires grown at low temperature

Cite as: J. Appl. Phys. **118**, 095702 (2015); https://doi.org/10.1063/1.4929821
Submitted: 12 May 2015 . Accepted: 18 August 2015 . Published Online: 01 September 2015

V. Zannier, T. Cremel, A. Artioli, D. Ferrand, K. Kheng, V. Grillo, and S. Rubini

View Online Export Citation CrossMark

ARTICLES YOU MAY BE INTERESTED IN

Dynamical properties and their strain-dependence of ZnSe(ZnSe:N): Zinc-blende and wurtzite
AIP Advances **4**, 067138 (2014); https://doi.org/10.1063/1.4885466

Zincblende-wurtzite phase transformation of ZnSe films by pulsed laser deposition with nitrogen doping
Applied Physics Letters **103**, 082111 (2013); https://doi.org/10.1063/1.4819271

Calculated natural band offsets of all II–VI and III–V semiconductors: Chemical trends and the role of cation d orbitals
Applied Physics Letters **72**, 2011 (1998); https://doi.org/10.1063/1.121249

Lock-in Amplifiers
Find out more today

Zurich Instruments

AIP Publishing

© 2015 AIP Publishing LLC.

Optical properties of single wurtzite/zinc-blende ZnSe nanowires grown at low temperature

V. Zannier,[1,2,a)] T. Cremel,[3,4,a)] A. Artioli,[3,5] D. Ferrand,[3,5] K. Kheng,[3,4] V. Grillo,[6,7] and S. Rubini[1]
[1]*IOM-CNR Laboratorio TASC, S. S. 14, Km. 163.5, I-34149 Trieste, Italy*
[2]*Department of Physics, University of Trieste, Via Valerio 2, I-34127 Trieste, Italy*
[3]*Univ. Grenoble Alpes, F-38000 Grenoble, France*
[4]*CEA, INAC-SP2M, « Nanophysique et Semiconducteurs » Group, F-38000 Grenoble, France*
[5]*CNRS, Institut Néel, « Nanophysique et Semiconducteurs » Group, F-38000 Grenoble, France*
[6]*IMEM-CNR, Parco Area delle Scienze 37/A, I-43010 Parma, Italy*
[7]*S3 NANO-CNR, Via Campi 213/A, I-41125 Modena, Italy*

(Received 12 May 2015; accepted 18 August 2015; published online 1 September 2015)

ZnSe nanowires with a dominant wurtzite structure have been grown at low temperature (300 °C) by molecular beam epitaxy assisted by solid Au nanoparticles. The nanowires emission is polarized perpendicularly to their axis in agreement with the wurtzite selection rules. Alternations of wurtzite and zinc-blende regions have been observed by transmission electron microscopy, and their impact on the nanowires optical properties has been studied by microphotoluminescence. The nanowires show a dominant intense near-band-edge emission as well as the ZnSe wurtzite free exciton line. A type II band alignment between zinc-blende and wurtzite ZnSe is evidenced by time-resolved photoluminescence. From this measurement, we deduce values for the conduction and valence band offsets of 98 and 50 meV, respectively. © *2015 AIP Publishing LLC*.
[http://dx.doi.org/10.1063/1.4929821]

I. INTRODUCTION

Semiconductor nanowires (NWs) have been increasingly studied in the past few years, both for fundamental research and applications in optoelectronics.[1] Among the many attractive properties they offer, the most peculiar one is the high surface/volume ratio, which has a profound effect on the crystal growth and can result in crystal structures not observed in the bulk. This effect has been observed for IV,[2] III-V,[3] and II-VI[4] semiconductor NWs. Moreover, the nanometer-sized diameter offers the opportunity for quantum confinement and for the growth of various axial and radial heterostructures.

ZnSe is a direct wide-band-gap II-VI semiconductor ($E_g = 2.7$ eV at 300 K), suitable for light emission in the blue-green region of the visible spectrum. One dimensional structures of ZnSe, such as NWs, nanorods, and nanoribbons, have been fabricated using a wide variety of growth techniques, and their potential applications in photodetectors,[5] sensors,[6] and lasers[7] have already been demonstrated. The stable crystal structure of ZnSe is zinc-blende (ZB), but it also occurs in the wurtzite (WZ) structure, metastable at room temperature and therefore difficult to obtain. Unlike the bulk case, ZnSe NWs often display WZ crystal structure, although the number of reports on ZB ZnSe NWs[8–11] exceeds those of WZ ones.[11,12] Periodically twinned ZnSe NWs with enhanced conductance have also been reported.[13] However, the photoluminescence of such twinned NWs was dominated by a broad deep-level (DL) emission between 500 and 650 nm, with a very weak (if not absent) near-band-edge (NBE) emission,[13,14] suggesting that twins and stacking faults have detrimental effects on the optical properties of ZnSe NWs. Thus, defect-free NWs are desirable to achieve good optical responses.[15,16]

To obtain good quality (single crystal) ZnSe NWs, the vapor-liquid-solid (VLS) mechanism has usually been exploited.[17] Indeed, it is well known that the VLS mechanism offers a good control over the NWs morphology, orientation, and crystal quality. Uniform arrays of long, straight, and well-oriented ZnSe NWs have been obtained using liquid catalyst particles to assist the growth.[18,19] However, it has been reported that some atoms of the liquid catalyst droplet can be incorporated as impurities along the wire's body, creating point defects that strongly affect their optical quality.[18,20] If solid particles are used in spite of liquid droplets, in the so-called vapor-solid-solid (VSS) mechanism, the probability of impurity atoms incorporations may be reduced and the optical properties of the NWs should be improved,[21–23] even though the control over the orientation, morphology, and crystal structure of VSS-grown NWs is not as easy as that of VLS-grown ones.[19,24]

In a recent paper,[23] some of us reported on the growth of vertically oriented ZnSe NWs by Au-assisted VSS growth on GaAs(111)B using molecular beam epitaxy (MBE). This study evidenced that a high growth temperature is detrimental on the NWs optical properties also in the case of VSS growth and that only NWs grown at temperature as low as 300 °C exhibit an enhanced NBE luminescence. However, a detailed optical characterization of those NWs is needed to relate their luminescence properties to their crystal structure. Here, we present a low-temperature microphotoluminescence (μPL) and cathodoluminescence (CL) study of

[a)]V. Zannier and T. Cremel contributed equally to this work.

 © 2015 AIP Publishing LLC

individual ZnSe NWs epitaxially grown on GaAs(111)B at 300 °C by MBE assisted by solid Au nanoparticles, and we correlate the optical response of the NWs with their crystal structure.

II. EXPERIMENTAL DETAILS

ZnSe NWs were grown by solid source MBE in a multi-chamber ultra-high-vacuum facility that includes individual chambers for III-V and II-VI semiconductor epitaxy as well as a metallization chamber for metal film deposition. The GaAs(111)B substrates were first deoxidized at 600 °C in the III-V chamber and then a 0.2 nm thick Au layer was deposited at room temperature in the metallization chamber. The substrates were finally transferred into the II-VI chamber where a 10 min annealing at 300 °C was followed by ZnSe deposition at the same temperature for 1 h. We used elemental Zn and Se sources, with fluxes corresponding to a two-dimensional ZnSe growth rate of 0.6 μm/h at 280 °C and a Zn/Se beam equivalent pressure ratio of 0.4. The NWs were characterized using a Zeiss SUPRA40 Scanning Electron Microscope (SEM). Transmission Electron Microscopy (TEM) was performed using a JEOL 2200 operated at 200 keV and with a Scherzer resolution in TEM and Scanning TEM (STEM) of 0.19 nm and 0.14 nm, respectively. The optical properties of both the as-grown sample and individual ZnSe NWs were investigated by low temperature (5 K) μPL and CL. For single-wire measurements, ZnSe NWs were first deposited on a patterned silicon substrate by gently rubbing the as-grown sample on the silicon surface. Isolated wires were identified and precisely located on the substrate by means of SEM. Low temperature spectra of the NWs were recorded using a cold-finger cryostat at 5 K and a confocal μPL setup. The NWs were excited with a 405 nm laser beam focused (1 μm diameter) on the selected NW using a microscope objective (NA = 0.6). The emitted light was collected by the microscope objective and sent to a spectrometer equipped with a CCD camera. For polarization measurements, a half-wave plate was rotated in front of a fixed linear polarizer placed before the spectrometer's entrance. CL images of the same NWs deposited on the silicon substrate were recorded using a FESEM FEI Inspect F50 (at 5 keV) equipped with a low temperature Gatan stage, to cool down the sample at 5 K, a high resolution IHR550 spectrometer, and a CL accessory.[25] The CL signal was collected by a parabolic mirror and sent to an avalanche photodiode detector synchronized with the electron beam scan. Time-resolved PL was performed on the as-grown sample using a Ti:sapphire laser exciting at 390 nm and a Hamamatsu C10910 streak camera. The laser-pulse width and the repetition rate were 200 fs and 76 MHz, respectively.

III. RESULTS AND DISCUSSION

In Figure 1, we show a representative SEM image of the as-grown GaAs(111)B substrate with ZnSe NWs obtained after 60 min of deposition at 300 °C. Straight and vertically oriented NWs (with the growth axis along the (111)B substrate direction) grew together with 3D non-catalyzed islands. The NWs have an average length of 1.8 μm and are strongly tapered, with a thick base (140–160 nm) and a thin tip (10–15 nm), roughly of the same size of the gold particle. Their pyramidal shape is a consequence of the low growth temperature which results in a low adatom mobility, i.e., in a substantial lateral growth.

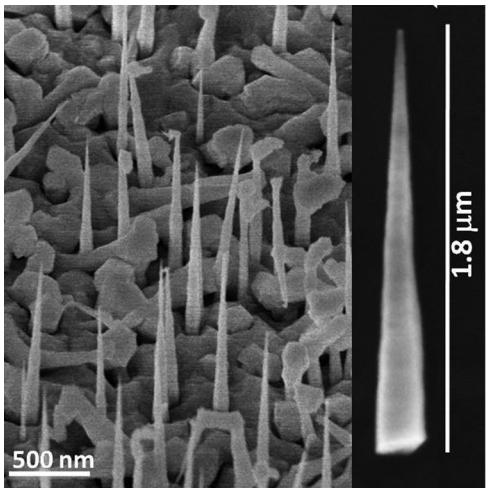

FIG. 1. Tilted-view SEM image (45°) of ZnSe NWs grown at 300 °C on GaAs(111)B. The inset on the right is a magnified image of a representative NW, mechanically transferred onto a Si wafer.

Even though the NWs have a quite homogeneous shape and morphology, TEM analysis (Figure 2) reveals the presence of different types of NWs: some of them have an almost defect-free WZ structure with the *c*-axis parallel to the

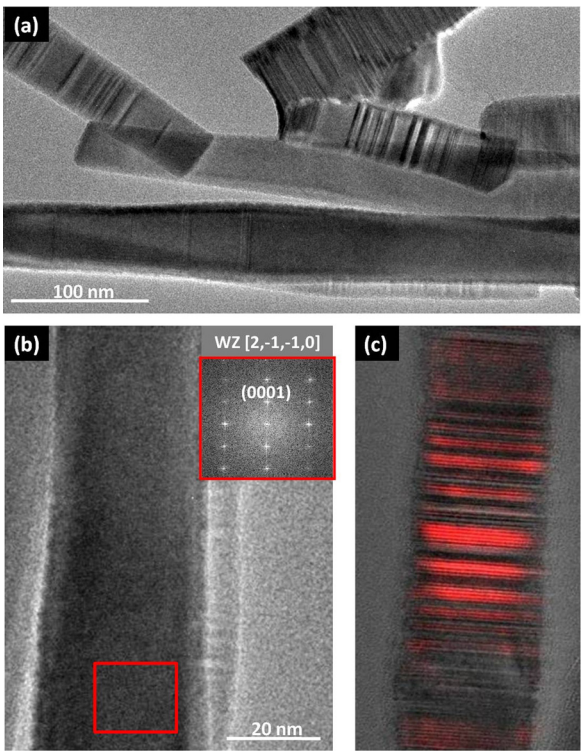

FIG. 2. TEM images of ZnSe NWs transferred on the TEM grid from the same as-grown sample. (a) Ensemble of NWs. (b) Representative image of a defect-free WZ NW. Inset: Fourier transform of the red rectangle on (b) highlighting the WZ structure of the NW (zone axis WZ [2,−1,−1,0]). (c) False-color HRTEM image of a NW with alternating WZ (red) and ZB crystal phases of various thickness.

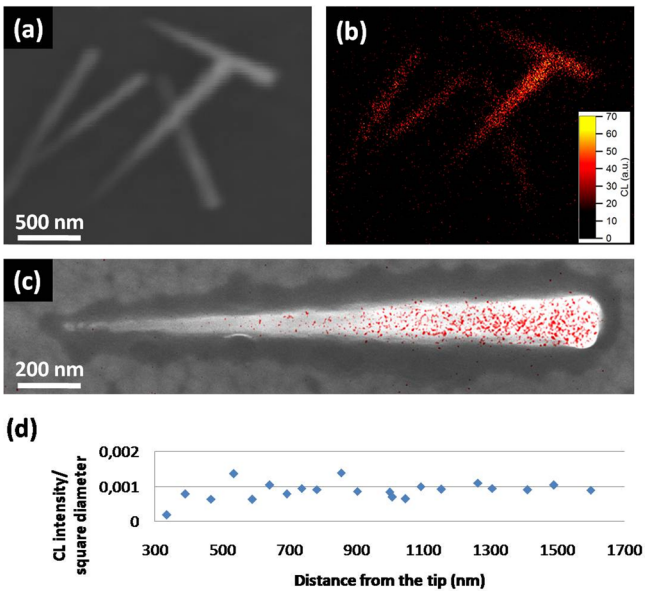

FIG. 3. (a) SEM image of a bundle of ZnSe NWs mechanically transferred from the as-grown sample onto a Si wafer. (b) CL image of the NWs shown in (a) recorded at 5 K. (c) Superimposition of the SEM image and the CL map (red pixels) of a ZnSe NW deposited on the Si wafer. (d) Plot of the CL intensity integrated across the NW diameter and divided by the NW square diameter, as a function of the position along the growth axis (distance from the tip) of the NW depicted in panel (c).

growth direction while others exhibit an alternation of WZ and ZB segments all along their body, with a variable thickness and periodicity. Figure 2(a) gives an overview of the different crystal quality of an ensemble of ZnSe NWs transferred from the same as-grown sample. Figure 2(b) shows a portion of the body of a pure WZ NW, whereas Figure 2(c) is a false-color HRTEM image taken along the body of another NW, where the alternation of WZ (red) and ZB regions is clearly visible.

Low temperature polychromatic CL images of the transferred NWs were recorded to assess the homogeneity of their optical properties. A CL emission was systematically detected from all the analyzed NWs, as shown in Figure 3. When an ensemble of NWs was imaged, the polychromatic map depicted the SEM image (Figures 3(a) and 3(b)), indicating that all the NWs are emitting light. Moreover, light is emitted all along the NWs body and the CL intensity increases from the tip to the base, as highlighted in Figure 3(c) which is a superimposition of the SEM image and the CL map of a single NW. In Figure 3(d), we report the plot of the CL intensity integrated across the NW diameter at different positions along its axis, divided by the square of the diameter, as a function of the distance from the tip. Such a ratio is a constant and it has already been observed in similarly tapered ZnTe NWs.[26] It indicates that the radiative efficiency remains constant along the NW body and the CL intensity is determined by the excitation density, proportional to the square diameter.

For small objects such as these NWs, the CL excitation efficiency is much lower than the PL one.[26] Indeed, an incident electron has a very small probability to be scattered inelastically and creates an electron-hole pair in the NW. As a result, this low excitation density prevents any spectral analysis of the CL signal of the NWs studied in this work. For this reason, we carried out low temperature PL measurements to analyze the NWs spectral response. Figure 4(a) shows that the NWs PL spectrum is dominated by a very intense NBE emission, within a range between 2.70 and 2.85 eV. No emission is found below 2.70 eV, indicating the absence of deep levels and donor-acceptor pair (DAP)

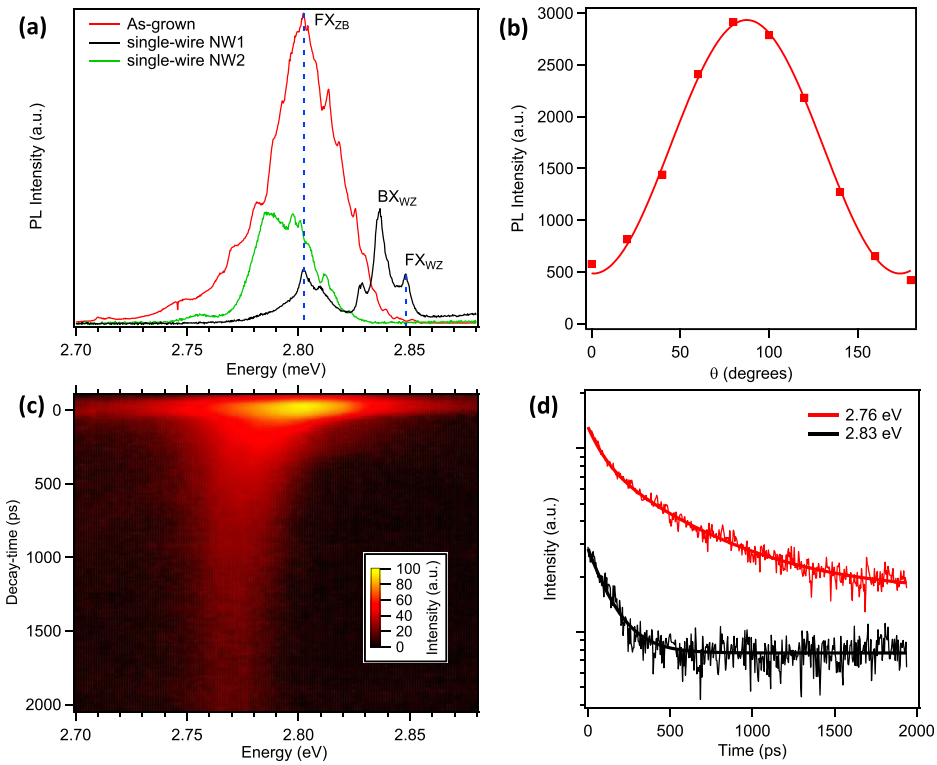

FIG. 4. (a) PL spectra of the as-grown sample and single NWs labelled NW1 and NW2 acquired at 5 K with a laser excitation of 30, 300, and 120 μW, respectively. (b) Circles: dependence of the intensity of the PL line FX$_{WZ}$ on the angle θ, between the NW1 axis and the direction of the linear polarization of the emitted light. Continuous line: Malus law fitting of the NW polarization. (c) As-grown sample decay-time map recorded with the streak camera. (d) Decay-time spectra of the PL lines at 2.76 (red) and 2.83 eV (black) measured on the as-grown sample.

recombination related to either impurity atoms[27–29] or extended structural defects known to occur in ZnSe crystals of both cubic[30] and hexagonal[31] structures. The presence of such deep level and DAP emission has been found also in the PL of ZnSe NWs grown by MBE at higher temperature[15,23] and with other deposition techniques.[32–35] Our results indicate that low temperature VSS-grown ZnSe NWs obtained by Au-assisted MBE have a superior optical quality. Indeed, we believe that the low growth temperature together with the solid state of the Au nanoparticle catalyst reduces the incorporation of impurities and the formation of thermally activated defects along the NWs, improving their NBE emission. The as-grown sample shows a broad band centered at 2.802 eV—ascribed to the ZB ZnSe free exciton recombination expected at 2.800 eV and labelled FX_{ZB} in Figure 4(a)[36]—with a full width at half maximum (FWHM) of 35 meV (red curve in Figure 4(a)). Single-NW spectra of two distinct ZnSe NWs are also reported in Figure 4(a). Some differences in peak shapes are found from wire to wire and explain the broadening of the as-grown-sample PL where an array of NWs is measured. Some NWs, as the one labelled NW1 in Figure 4(a) (which is also the NW studied in Figure 3(c)), exhibit few narrow lines above the band gap of ZB ZnSe (2.820 at 6 K). Saxena *et al.*[36] reported on the PL of pure WZ ZnSe NWs showing a spectrum characterized by the presence of a broad DAP peak at 2.747 eV and two narrow lines at 2.841 and 2.833 eV, respectively. Those peaks were attributed to the exciton bound to neutral acceptors involving Zn-vacancies and Zn-vacancies complexes, with a calculated dissociation energy (defined as the energy difference between the free and the bound exciton emission) of 11 and 19 meV, respectively. In our case, NW1 shows three well defined peaks above the ZB band gap: a narrow line at 2.848 eV, a most intense line centered at 2.837 eV, and a weak line at 2.829 eV. We speculate that the line at 2.848 eV, which is close to the highest energy peak reported by Liang and Yoffe at 2.851 eV,[31] is the free A exciton emission in the WZ phase, thus labelled FX_{WZ} in Figure 4(a). The other two lines at lower energy can be attributed to recombinations of excitons bound to neutral acceptors of the same nature of what is reported in Ref. 36; the most intense one is labelled BX_{WZ}. Even though this interpretation is not straightforward, the presence of Zn-vacancies in the NWs is probable due to the Se-rich growth conditions used during the growth.

Figure 4(b) displays the intensity variation of the NW1 FX_{WZ} line when rotating the linear polarization of the detection with respect to the NW axis. The maximum of the emission intensity is reached when the polarization is perpendicular to the NW axis ($\theta = 90°$). The polarization ratio of the lines BX_{WZ} and FX_{WZ} is $78 \pm 3\%$, and this behavior has been observed on other NWs. This uncommon result can be understood taking into account the prevalent WZ crystal structure of these NWs. Usually, optical absorption and PL of NWs are polarized parallel to the NW axis because of the large dielectric contrast between the NW and its environment: the electric field inside the cylinder is attenuated when the incident field is polarized perpendicular to the cylinder because the exciting wavelength is larger than the wire diameter.[37] Indeed, NWs with a ZB crystal structure normally show a strongly polarized PL parallel to the wire axis.[37–40] In WZ semiconductors, the crystal field and the spin-orbit interaction split the top valence band into Γ_9(A), Γ_7(B), and Γ_7(C) states and introduce some selection rules. The lowest energy optical transition (between the valence Γ_9(A) state and the lowest conduction Γ_7 state) is allowed only for light polarization perpendicular to the [0001] *c*-axis,[41] and this behavior has been observed in bulk WZ ZnSe crystals.[31] This explains the polarization perpendicular to the growth axis (which is the *c*-axis of the WZ structure) observed for our NWs.

As also found for WZ NWs of other materials,[39,42,43] the degree of polarization is lower in WZ (polarization $\perp$ to the NW axis) compared to ZB NWs (polarization // to the NW axis). A quantitative explanation of this polarization reduction in a WZ NW requires a more complicated calculation. Ruda and Shik[44] demonstrate that the NW polarization in *emission* depends on the NW diameter. According to their calculation, an isotropic (unpolarized) internal emission in a NW of diameter 100 nm (diameter of our NW base from which the light is mainly emitted) has an external polarization of 23% along its axis. This can explain why we did not observe a fully polarized emission but a 78% polarization perpendicular to the NW axis.

The peculiar polarization properties of these ZnSe NWs make them attractive for photonic applications, especially as single photon sources.[45] In NWs with perpendicularly polarized PL, the exciton or electron-hole pair can be seen as a dipole oriented perpendicularly to the NW *c*-axis; the dipole is said to be orthogonal. Such an orthogonal dipole is highly efficient in photon extraction along the NW axis.[46] While a dipole oriented along the photonic wire axis degrades the photon extraction efficiency, an orthogonal dipole is a necessary condition to reach the highest achievable photon extraction.[47]

NW1 and NW2 also show a peak at the FX_{ZB} energy of 2.800 eV, and most of the analyzed NWs show only a rather broad emission between 2.788 and 2.816 eV (see NW2 in Figure 4(a)). This band includes the excitonic lines of ZB ZnSe known to appear between 2.780 and 2.800 eV,[11] but also interband transitions occurring at the WZ/ZB interfaces. Indeed, it has been shown by the TEM analysis (Figure 2) that many of these NWs present an alternation of WZ and ZB portions all along their body. ZB ZnSe has a smaller band gap and large negative band offset respect to WZ ZnSe.[48] Hence, the WZ/ZB interface gives a type II alignment, with the conduction and the valence bands of the ZB segments lower than those of the WZ portion. At the interface, electrons are confined in the ZB region and holes in the WZ region of the NW; their recombination will result in emission lines at a lower energy than the ZB bandgap (see the schematic diagram in Figure 5). Moreover, a short ZB section into a WZ crystal defines a quantum well. In a NW, such a structure forms in a crystal phase quantum dot.[49,50] The ZB segment length sets the confined electron energy levels, therefore when ZB insertions of different thickness are present in the same WZ matrix, as for these NWs, the PL spectrum will be composed of a broad band instead of a few

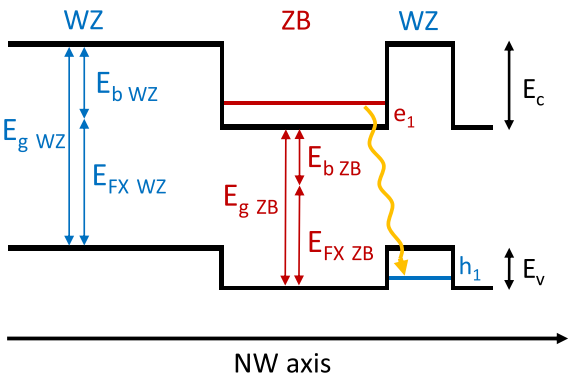

FIG. 5. Illustration of the band profile and transitions in a ZnSe WZ and ZB heterostructure.

narrow lines. If WZ sections are also short, confined energy levels will be found also for holes in the WZ phase increasing the range of the spectral emission.

Spatially indirect e-h recombinations are expected to be characterized by longer lifetimes, due to the reduced overlap of the electron and hole wave functions.[49] Figure 4(c) is a decay-time map of ZnSe NWs (the as-grown sample) recorded with the streak camera, which shows the time evolution of the PL after excitation by the Ti:Sapphire pulsed laser. The low-energy peaks (from 2.75 ± 0.01 eV to 2.79 ± 0.01 eV) present a longer tail signal than the high-energy peaks (from 2.80 to 2.86 eV). Indeed, as shown in Figure 4(d), the lifetime of the high energy PL line at 2.83 eV is 140 ± 10 ps (fitted with a monoexponential plus a constant for the background). Besides, the low energy peak at 2.76 eV has a non-monoexponential behavior with a lifetime longer than 1.7 ± 0.2 ns (fitted with a biexponential) presented in Figure 4(d). For this low energy peak, the detection of photons after 2000 ps highlights slow electron-hole pairs recombinations dynamic. This measurement reinforces our hypothesis that the lower energy peaks are due to spatially indirect recombinations in type II heterostructures.

Moreover, we can notice in Figure 4(c) that, at time $t = 0$, the type-II emission lines are blue-shifted due to Stark effect. This phenomenon is induced by band bending (at low carriers concentration) and band filling (at high carriers concentration) created by the electron/hole pairs separation at the heterostructure interface.[51] Then, we observe a PL redshift as a function of time due to the reduction of the Stark effect, while the electron-hole pairs progressively recombine. This is why the type II recombinations in Figure 4(c) have the shape of an inverted comma.

While the TEM analysis has shown that the prevalent NWs structure is WZ, the PL spectrum of the as-grown sample shows only a slight emission at the energy of WZ ZnSe free exciton (2.848 eV). This result can be explained by the low excitation power of 30 μW used to excite the as-grown sample (see supplementary material[52] to notice that, at a high enough laser power, the WZ ZnSe free exciton is visible). Indeed, when the excitons are created in the mainly but not completely WZ NWs, they diffuse within the NW and encounter a ZB NW segment. According to Figure 5, the electrons will be trapped within the ZB segment, while the holes will remain in the WZ part and type II recombination will occur. In order to observe the luminescence from the WZ part—as for NW1 excited with a laser power of 300 μW—we first need to saturate the ZB segments. To conclude, we observe a long decay-time within the energy range from 2.75 ± 0.01 eV to 2.79 ± 0.01 eV, and we assume that these transitions correspond to type II recombinations.

To go further with the analysis of the ZnSe WZ/ZB alternations, we can estimate values for their conduction and valence band offsets. We expect the recombination energy for the type II transition (see orange arrow in Figure 5) to be given by

$$E_{type\,II} = E_{FX_{ZB}} + (E_{b_{ZB}} - E_{b_{ind}}) + e_1 + h_1 - \Delta E_V,$$

with $E_{FX_{ZB}}$ the ZB ZnSe free exciton energy of 2.800 eV, $E_{b_{ZB}}$ and $E_{b_{ind}}$ are the exciton binding energy for ZB (21 meV (Ref. 35)) and the type II indirect recombination, respectively, e_1 and h_1 are the electron and hole confinement energy, and ΔE_V is the valence band offset (see Figure 5). We neglect the binding energy difference $(E_{b_{ZB}} - E_{b_{ind}})$ due to their small and expected similar values, as well as piezoelectric effects due to the small lattice mismatch of 0.7% between ZB and WZ ZnSe segments.

If the experimentally observed transitions are due to type II recombinations in ZB/WZ crystal phase heterostructures, the lowest emission energy should correspond to interface recombinations without confinement effects. The conduction and valence band-offsets at the interface are $\Delta E_C = E_{FX_{WZ}} - E_{type\_II}$ and $\Delta E_V = E_{FX_{ZB}} - E_{type\_II}$, respectively ($E_{FX_{WZ}} = 2.848$ eV). According to the decay-time measurements and as discussed above, the lowest type II recombination energy is at 2.75 ± 0.01 eV. Therefore, we estimate an upper limit for the valence and the conduction band-offsets to be 50 ± 10 meV and 98 ± 10 meV, respectively.

On the other extreme, the shortest period of a ZB/WZ alternation should give the highest recombination energy, due to the presence of confined states for holes in ZB and for electrons in WZ. According to Caroff *et al.*,[53] the smallest possible ZB and WZ portions within a NW are composed of three and four bilayers along the ZB (111) or WZ *c*-axis. Therefore along this growth direction, the smallest ZB and WZ portions have a length of 1.96 and 2.62 nm, respectively. Assuming the ZnSe electron and hole masses along (111) to be 0.16 and 1.09 m_0,[54] we calculate the confined states and determine the higher energy limit of the type II recombinations to be 2.84 ± 0.01 eV, quite close to the highest energy transition (2.80 eV) attributed to type II recombinations in Figure 4(c). The calculated energy overestimation is probably due to the use of the ZB (111) hole mass for the calculation because the WZ structure value is unknown. Another possible reason is the formation of minibands caused by the electron and hole wave functions overlap that reduce the confinement energy when there is a high density of short ZB and WZ portions.[50]

IV. CONCLUSIONS

To summarize, we presented a combined structural and optical characterization of ZnSe NWs grown at 300 °C by

MBE. TEM analysis reveals the presence of NWs with pure WZ structure together with NWs with alternations of WZ and ZB phase. The NWs show an excellent optical quality, with a dominant near-band-edge emission where the ZnSe WZ free exciton line can be identified. The polarization of the emitted light is found perpendicular to the NW axis, in agreement with what is expected considering the dominant WZ structure. This peculiar light polarization of the WZ NWs opens the way to their application in single photon sources. Moreover, single-NW CL images show a homogeneous radiative efficiency along the NW body despite the presence of mixed phase regions. Using time-resolved PL, we revealed a type II band alignment between ZB and WZ ZnSe and deduced the conduction and valence band offsets to be 98 and 50 meV, respectively. The experimental estimation of these values will be useful in the design of ZnSe structural quantum dot NWs where portions of ZB are introduced in WZ NWs as soon as a precise control of the NW structure by means of the growth conditions will be achieved.

ACKNOWLEDGMENTS

We thank Dr. Jean-Michel Gérard, Dr. Bruno Gayral, Dr. Vladimir Kochereshko, Dr. Joël Cibert, and Dr. Régis André for stimulating discussions. We acknowledge Dr. Petr Stepanov, Dr. Joël Bleuse, and Dr. Fabrice Donatini for their help during the time-resolved and cathodoluminescence measurements. V.Z. acknowledges support by Campus France-Ministère des Affaires Etrangères.

[1]T. J. Kempa, S. Kim, R. W. Day, H. Park, D. G. Nocera, and C. M. Lieber, J. Am. Chem. Soc. **135**, 18354 (2013).
[2]P. B. Sorokin, P. V. Avramov, V. A. Demin, and L. A. Chernozatonskii, J. Exp. Theor. Phys. Lett. **92**, 352 (2010).
[3]P. Kusch, E. Grelich, C. Somaschini, E. Luna, M. Ramsteiner, L. Geelhaar, H. Riechert, and S. Reich, Phys. Rev. B **89**, 045310 (2014).
[4]P. Rueda-Fonseca, E. Bellet-Amalric, R. Vigliaturo, M. den Hertog, Y. Genuist, R. André, E. Robin, A. Artioli, P. Stepanov, D. Ferrand, K. Kheng, S. Tatarenko, and J. Cibert, Nano Lett. **14**, 1877 (2014).
[5]X. Fang, S. Xiong, T. Zhai, Y. Bando, M. Liao, U. K. Gautam, Y. Koide, X. Zhang, Y. Qian, and D. Golberg, Adv. Mater. **21**, 5016 (2009).
[6]Y. P. Leung, W. C. H. Choy, and T. I. Yuk, Chem. Phys. Lett. **457**, 198 (2008).
[7]G. Xing, J. Luo, H. Li, B. Wu, X. Liu, C. Hon, A. Huan, H. J. Fan, and T. C. Sum, Adv. Opt. Mater. **1**, 319 (2013).
[8]Y. F. Chan, X. F. Duan, S. K. Chan, I. K. Sou, X. X. Zhang, and N. Wang, Appl. Phys. Lett. **83**, 2665 (2003).
[9]S. K. Chan, Y. Cai, I. K. Sou, and N. Wang, J. Cryst. Growth **278**, 146 (2005).
[10]C. Fernandes, H. Ruda, A. Saxena, and C. De Souza, Phys. Status Solidi C **9**, 2460 (2012).
[11]A. Saxena, Q. Pan, and H. E. Ruda, Nanotechnology **24**, 105701 (2013).
[12]C. X. Shan, Z. Liu, X. T. Zhang, C. C. Wong, and S. K. Hark, Nanotechnology **17**, 5561 (2006).
[13]X. Fan, X. M. Meng, X. H. Zhang, M. L. Zhang, J. S. Jie, W. J. Zhang, C. S. Lee, and S. T. Lee, J. Phys. Chem. C **113**, 834 (2009).
[14]Y. Q. Wang, U. Philipose, T. Xu, H. E. Ruda, and K. L. Kavanagh, Semicond. Sci. Technol. **22**, 175 (2007).
[15]T. Aichele, A. Tribu, C. Bougerol, K. Kheng, R. André, and S. Tatarenko, Appl. Phys. Lett. **93**, 143106 (2008).
[16]T. Aichele, A. Tribu, C. Bougerol, K. Kheng, F. Donatini, L. S. Dang, R. André, and S. Tatarenko, Phys. Status Solidi B **246**, 812 (2009).
[17]K. B. Kahen, I. A. Goldthorpe, and J. Minter, J. Cryst. Growth **322**, 57 (2011).
[18]Y. Liang, Y. Tao, and S. K. Hark, CrystEngComm **13**, 5751 (2011).
[19]V. Zannier, V. Grillo, F. Martelli, J. R. Plaisier, A. Lausi, and S. Rubini, Nanoscale **6**, 8392 (2014).
[20]E. Carlino, F. Martelli, S. Rubini, and A. Franciosi, Philos. Mag. Lett. **86**, 261 (2006).
[21]E. Bellet-Amalric, M. Elouneg-Jamroz, P. Rueda-Fonseca, S. Bounouar, M. Den Hertog, C. Bougerol, R. André, Y. Genuist, J.-P. Poizat, K. Kheng, J. Cibert, and S. Tatarenko, J. Cryst. Growth **378**, 233 (2013).
[22]S. Bounouar, M. Elouneg-Jamroz, M. Den Hertog, C. Morchutt, E. Bellet-Amalric, R. André, C. Bougerol, Y. Genuist, J.-P. Poizat, S. Tatarenko, and K. Kheng, Nano Lett. **12**, 2977 (2012).
[23]V. Zannier, F. Martelli, V. Grillo, J. R. Plaisier, A. Lausi, and S. Rubini, Phys. Status Solidi RRL **8**, 182 (2014).
[24]V. Zannier, V. Grillo, and S. Rubini, J. Phys. D: Appl. Phys. **47**, 394005 (2014).
[25]F. Donatini and L. S. Dang, Nanotechnology **21**, 375303 (2010).
[26]A. Artioli, P. Rueda-Fonseca, P. Stepanov, E. Bellet-Amalric, M. Den Hertog, C. Bougerol, Y. Genuist, F. Donatini, R. André, G. Nogues, K. Kheng, S. Tatarenko, D. Ferrand, and J. Cibert, Appl. Phys. Lett. **103**, 222106 (2013).
[27]M. Yamaguchi, A. Yamamoto, and M. Kondo, J. Appl. Phys. **48**, 5237 (1977).
[28]P. J. Dean and D. C. Herbert, Phys. Rev. B **23**, 4888 (1981).
[29]A. D. Raisanen, L. J. Brillson, L. Vanzetti, A. Bonanni, and A. Franciosi, Appl. Phys. Lett. **66**, 3301 (1995).
[30]T. Taguchi, T. Kusao, and A. Hiraki, J. Cryst. Growth **72**, 46 (1985).
[31]W. Liang and A. Yoffe, Philos. Mag. **16**, 1153 (1967).
[32]Y.-C. Zhu and Y. Bando, Chem. Phys. Lett. **377**, 367 (2003).
[33]U. Philipose, S. Yang, T. Xu, and H. E. Ruda, Appl. Phys. Lett. **90**, 063103 (2007).
[34]U. Philipose, A. Saxena, H. E. Ruda, P. J. Simpson, Y. Q. Wang, and K. L. Kavanagh, Nanotechnology **19**, 215715 (2008).
[35]A. Saxena, S. Yang, U. Philipose, and H. E. Ruda, J. Appl. Phys. **103**, 053109 (2008).
[36]A. Saxena, Q. Pan, and H. E. Ruda, Nanoscale **5**, 2875 (2013).
[37]J. Wang, M. S. Gudiksen, X. Duan, Y. Cui, and C. M. Lieber, Science **293**, 1455 (2001). Using the equation reported in this paper, the theoretical absorption polarization ratio of ZB ZnSe NWs is 92% parallel to the wire axis (ZB ZnSe refractive index of 2.98 at 440 nm interpolated from the equation reported in Ref. 38).
[38]J. Connolly, B. diBenedetto, and R. Donadio, "Specifications of Raytran material," Proc. SPIE **181**, 141–144 (1979).
[39]A. Mishra, L. V. Titova, T. B. Hoang, H. E. Jackson, L. M. Smith, J. M. Yarrison-Rice, Y. Kim, H. J. Joyce, Q. Gao, H. H. Tan, and C. Jagadish, Appl. Phys. Lett. **91**, 263104 (2007).
[40]T. L. Spencer, R. Cisek, V. Barzda, U. Philipose, H. E. Ruda, and A. Shik, Appl. Phys. Lett. **94**, 233119 (2009).
[41]J. Birman, Phys. Rev. Lett. **2**, 157 (1959).
[42]Y. Masumoto, Y. Hirata, P. Mohan, J. Motohisa, and T. Fukui, Appl. Phys. Lett. **98**, 211902 (2011).
[43]T. Ba Hoang, A. F. Moses, L. Ahtapodov, H. Zhou, D. L. Dheeraj, A. T. J. van Helvoort, B.-O. Fimland, and H. Weman, Nano Lett. **10**, 2927 (2010).
[44]H. E. Ruda and A. Shik, J. Appl. Phys. **100**, 024314 (2006).
[45]J. Claudon, N. Gregersen, P. Lalanne, and J.-M. Gérard, ChemPhysChem **14**, 2393 (2013).
[46]T. Cremel, M. Elouneg-Jamroz, E. Bellet-Amalric, L. Cagnon, S. Tatarenko, and K. Kheng, Phys. Status Solidi C **11**, 1263 (2014).
[47]J. Claudon, J. Bleuse, N. S. Malik, M. Bazin, P. Jaffrennou, N. Gregersen, C. Sauvan, P. Lalanne, and J.-M. Gérard, Nat. Photonics **4**, 174 (2010).
[48]M. Murayama and T. Nakayama, Phys. Rev. B **49**, 4710 (1994).
[49]N. Akopian, G. Patriarche, L. Liu, J.-C. Harmand, and V. Zwiller, Nano Lett. **10**, 1198 (2010).
[50]D. Spirkoska, J. Arbiol, A. Gustafsson, S. Conesa-Boj, F. Glas, I. Zardo, M. Heigoldt, M. H. Gass, A. L. Bleloch, S. Estrade, M. Kaniber, J. Rossler, F. Peiro, J. R. Morante, G. Abstreiter, L. Samuelson, and A. Fontcuberta i Morral, Phys. Rev. B **80**, 245325 (2009).
[51]J. Bao, D. C. Bell, F. Capasso, J. B. Wagner, T. Martensson, J. Tragardh, and L. Samuelson, Nano Lett. **8**, 836 (2008).
[52]See supplementary material at http://dx.doi.org/10.1063/1.4929821 for a figure showing that at a high enough laser excitation power, the wurtzite ZnSe free exciton line appears at 2.85 eV.
[53]P. Caroff, K. A. Dick, J. Johansson, M. E. Messing, K. Deppert, and L. Samuelson, Nat. Nanotechnol. **4**, 50 (2009).
[54]Springer Materials, the Landolt-Börnstein Database.